

## Crystal Chemistry and Physical Properties of the Non-Magnetic Kondo-Compound $\text{HfAs}_{1.7}\text{Se}_{0.2}$

Andreas Schlechte, Gudrun Auffermann, Michal Bednarski<sup>1</sup>, Łukasz Bochenek<sup>1</sup>, Maik Böhme, Tomasz Cichorek<sup>1</sup>, Rainer Niewa<sup>2</sup>, Niels Oeschler, Marcus Schmidt, Frank Steglich, and Rüdiger Kniep

### Introduction

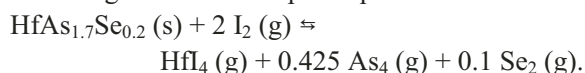
This joint project is devoted to the investigation of the correlation of structural phenomena and physical properties, especially with regard to the non-magnetic Kondo effect. The chemical systems we concentrated on are the pnictide-chalcogenides crystallizing in the PbFCl structure (or variants of this type of structure). Our recent investigations of the structurally disordered systems Zr–As–Se and Th–As–Se already pointed out the relevance of structural two-level systems (TLS) for electronic transport on a macroscopic scale [1-3]. Whereas the low- $T$  properties provide clear evidence for the presence of tunneling centers, the electrical resistivity  $\rho(T)$  shows an anomalous upturn upon cooling below 16 K. Most importantly, however, the  $T^{1/2}$  amplitude is unaffected by strong magnetic fields. Such a behavior is a hallmark of a non-magnetic Kondo effect derived from structural two-level systems. In the respective Hf system we succeeded only recently in the synthesis of  $\text{HfAs}_{1.7}\text{Se}_{0.2}$  [4]. This system exemplifies the close chemical, physical, and crystallographic relations between zirconium- [5,6], cerium- [7], and thorium-arsenide-selenides [8,9].

The intensively studied metallic phase  $\text{ZrAs}_{1.4}\text{Se}_{0.5}$  crystallizes in the ZrSiS (PbFCl) type of structure, with vacancies within the arsenic layers and As–Se mixed occupations. On the other hand, CeAsSe crystallizes in a distorted variant of the ZrSiS aristotype, with fully occupied positions and no significant mixed-site occupations. The distortion occurs due to the formation of infinite cis-trans chains of arsenic atoms. The differences between the ternary Zr and Ce systems may be traced back to different electronic situations of the metal atoms ( $\text{Zr}^{+4}$  and  $\text{Ce}^{+3}$ , respectively).

Substitution of zirconium by hafnium again leads to an arsenic-rich compound,  $\text{HfAs}_{1.7}\text{Se}_{0.2}$ , which contains vacancies within the arsenic layers and mixed occupancy of the As/Se positions as also present in the Zr-phase. Physical and chemical properties of  $\text{HfAs}_{1.7}\text{Se}_{0.2}$  [4] and  $\text{ZrAs}_{1.4}\text{Se}_{0.5}$  [2] are closely related.

### Synthesis and Crystal Growth

Large single crystals (up to  $5 \times 2 \times 1 \text{ mm}^3$ ) of  $\text{HfAs}_{1.7}\text{Se}_{0.2}$  were synthesized from prereacted elemental powders via exothermal chemical transport using iodine as transport agent. The temperature gradient from 1073 K (source) to 1173 K (crystal growth side) was chosen based on results from difference scanning calorimetry (DSC, NETZSCH 404C), difference thermal analysis / thermogravimetry (DTA/TG, NETZSCH STA 449C), and from thermodynamic calculations. The reaction of a cold-pressed mixture of the respective elements is completed with the formation of the ternary phase (DSC) at 1023 K. This phase decomposes under Ar (without melting) at about 1200 K into binary HfAs (DTA/TG) as the major solid decomposition product. Preliminary thermodynamic evaluations approximately lead to the following chemical transport equilibrium:



The gaseous phases were determined via mass spectrometry. Thermodynamic calculations reveal a strong negative enthalpy of reaction, confirming the exothermic character of the transport reaction.

For preparation of the previously investigated compound,  $\text{ZrAs}_{1.4}\text{Se}_{0.5}$ , sealable glassy carbon tubes were used to prevent reactions with the tube material such as fused silica [1]. This experimental setup has one main disadvantage with regard to chemical transport reactions: a smeared temperature gradient that reduces the transport efficiency. Therefore, the chemical transport reactions were carried out in carbon-coated fused silica ampoules (coating by pyrolysis of acetone). This procedure ensured that the source materials as well as the growing crystals do not directly get in contact with the fused-silica ampoule, and the temperature gradient is clearly sharpened.

## Chemical Characterization

The chemical composition of the crystals under investigation was determined by electron-probe micro-analyses with wavelength-dispersive X-ray spectroscopy (WDXS, Cameca SX 100) as well as by chemical analyses applying the ICP–OES method (inductively-coupled-plasma–optical-emission-spectrometry). Silicon as conceivable impurity (from the tube material) was quantified by LA–ICP–MS (laser-ablation–inductively-coupled-plasma–mass-spectrometry). In addition, combustion ion chromatography (CIC) was applied to detect possible contaminations by iodine which was used as transport agent. The presence of small amounts of para- (equivalent to  $\leq 200$  wt. ppm ions with  $S = \frac{1}{2}$ ) and ferromagnetic (equivalent to  $\leq 10$  wt. ppm Fe metal) impurities was indicated by magnetic susceptibility measurements.

A selected part of one of the grown single crystals (Fig. 1) was cut by means of a wire saw, embedded plane-parallel into Polyfast, and polished for WDXS measurements.

The larger part of this single crystal was designated for measurements of the physical properties. WDXS measurements on the smaller fragment did not give any evidence for inhomogeneities or impurities, with the exception of silicon. For quantitative analyses, a ternary Zr–As–Se standard for arsenic/selenium and an elemental Hf standard were used. The atomic ratio of the respective elements lead on average (ten measuring points) to Hf: 35.23(9) at.%, As: 57.2(1) at.%, and Se: 7.55(5) at.%, which results in the formula  $\text{Hf}_{1.000(3)}\text{As}_{1.624(3)}\text{Se}_{0.214(1)}$  (normalized to Hf).

In addition, several crystals of  $\text{HfAs}_{1.7}\text{Se}_{0.2}$  were quantitatively analyzed with ICP–OES (Vista RL, Varian) concerning the three main components. A digestion procedure was optimized for the specific Hf–As–Se system. Accurate and reproducible results were achieved by application of the closed

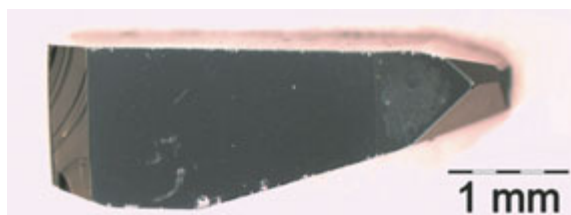


Fig. 1: Light-microscopic image of a single crystal  $\text{HfAs}_{1.7}\text{Se}_{0.2}$ .

vessel pressure microwave decomposition procedure (ETHOS plus 2, MLS). Optimized reaction conditions were derived as follows: Seven accurately ( $\pm 0.001$  mg) weighed samples (5 to 8 mg) were decomposed individually in an acid mixture of 2.5 mL  $\text{HNO}_3$  (65%) and 0.5 mL HF (40%) at a temperature of 423 K for 10 min. The solutions were completely transferred into volumetric flasks (50 mL) and filled up with ultra-pure water. Subsequently, they were measured against a matrix-matched standard calibration series. The analytical results did not show any indication of inhomogeneities of different crystals taken from the same batch and led to the formula  $\text{Hf}_{1.000(2)}\text{As}_{1.66(2)}\text{Se}_{0.215(5)}$ . The contamination of the samples with regard to other metals was investigated by ICP–OES, revealing values below the respective limits of detection (apart from Fe and Zr: 0.1 and 0.15 wt.%, respectively). Additionally, several crystals were checked for oxygen and carbon impurities by means of the carrier gas hot extraction and the combustion methods (TCH600 and C200, LECO). The measured values were below the limits of detection,  $\leq 0.1$  and 0.03 wt.%, respectively. An always crucial question is whether a sample is contaminated with components from the tube material. In this context the single crystals were also checked with regard to their content of Si impurities. To pursue this issue we decided to use the LA–ICP–MS setup, which is a powerful tool for the quantitative analysis of traces in materials, especially concerning their spatial and depth distribution. Additionally, and in contrast to the aforementioned methods, this technique is nearly non-destructive and provides the opportunity for further studies after elemental analysis of the crystal. The investigations were carried out with the laser ablation system Geoloas Q Plus (Coherent) connected with an ICP–MS 810 (Varian). The used wavelength of 193 nm (ArF Excimer Laser Complex 102, Coherent) allowed a well defined ablation with spot sizes in the range of 5 – 150  $\mu\text{m}$  in diameter. Quantitative results were obtained by using a reference standard (NIST 610) and Hf as internal standard. The studies were evaluated with regard to the given problem in order to increase the precision and the accuracy of the method. The investigations were finally carried out on six crystals from one batch using He as carrier gas. The extensive studies led to an optimization of the ablation process. Five different spots of 100  $\mu\text{m}$  in

diameter on each crystal were ablated by 50 pulses with an energy density of  $10 \text{ J/cm}^2$  and a repetition rate of 1 Hz. The analytical quantification parameters revealed that the sample contained significant amounts of Si (0.94(5) wt.%), nearly homogeneously distributed over the whole crystal. This resulted in an overall composition of  $\text{Hf}_{1.000(2)}\text{As}_{1.66(2)}\text{Se}_{0.215(1)}\text{Si}_{0.108(5)}$ . The images of the ablation craters were recorded with a profilometer PL $\mu$  (Atos) and by scanning electron microscopy (ESEM Quanta 200 F, FEI Company) operated in a high-vacuum mode and at an acceleration voltage of 30 kV (Fig. 2).

In addition, the crystals were checked with regard to the transport agent (iodine). In 2008, an oxidative combustion system in conjunction with an ion chromatography (CIC) setup (AQF-100, GA-100, WS-100: Mitsubishi Chemical, a<sup>1</sup> envirotech; ICS-1000: Dionex) was established in our institute. This setup enables us to analyze the content of halides (F, Cl, Br, I) quantitatively and even simultaneously in solid materials. With respect to our specific problems the two main advantages of this method are given by (i) the solid phase pyrolysis as the decomposition method and (ii) the low limits of detection for the halide impurities in a sample (the quantitative determination of halides as main components is also possible with high precision). Thus, this method is independent of both the sample matrix and the risk of substantial changes of the solutions during the measurement procedure. The combustion ion chromatography (CIC) equipment consists of a quartz-tube high-temperature furnace in which the sample is stepwise inserted by control of a computer program. This ensures that the temperature region is optimally adapted to the reactivity of the sample under investigation. The furnace outlet is directly coupled to a gas absorbing unit where the gases are passed through an absorption solution. Here, the acidic components are trapped in an aqueous solution containing an internal standard. Finally, the absorption solution is automatically injected into the ion chromatography (IC) unit for quantitative analysis. For the quantitative determination of iodine, 5 – 10 mg of  $\text{HfAs}_{1.7}\text{Se}_{0.2}$  were stepwise heated in a stream of  $\text{Ar/O}_2$  up to 1275 K.

The formed gaseous products were absorbed in a solution containing  $\text{SO}_4^{2-}$  as internal standard. The latter was used to avoid an overlap with the signals caused by Se and As. The IC system was cali-

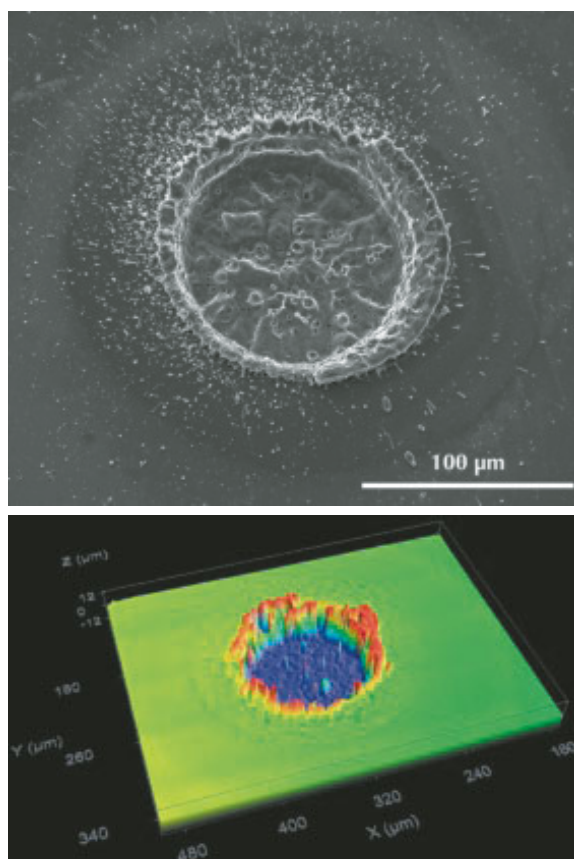


Fig. 2: Images of a crater formed by laser ablation on a  $\text{HfAs}_{1.7}\text{Se}_{0.2}$  crystal recorded by SEM (top) and by profilometry (bottom).

brated from 0 to 1 mg/L  $\Gamma$  by using freshly prepared standard solutions. The analytical results from five independent measurements did not reveal any impurities of iodine in the sample (limit of detection: 0.02 wt.%).

### Crystal Structure

$\text{HfAs}_{1.7}\text{Se}_{0.2}$  crystallizes in the  $\text{ZrSiS}$  (PbFCl) type of structure with  $a = 370.841(5) \text{ pm}$ , and  $c = 804.96(1) \text{ pm}$  (295 K). In this crystal structure the arsenic layer  $\text{As}_{0.90(1)}$  contains vacancies on site  $2a$ . The absence of unusual displacement parameters for arsenic ( $2a$ ) indicates differences in the bonding situation compared to  $\text{ZrAs}_{1.4}\text{Se}_{0.5}$ . The displacement of the arsenic atoms in the square-planar As-layer in  $\text{ZrAs}_{1.4}\text{Se}_{0.5}$  is significantly larger compared with  $\text{HfAs}_{1.7}\text{Se}_{0.2}$ . The remaining arsenic atoms together with the selenium atoms occupy the position  $2c$  and form a mixed occupied site  $\text{As}_{0.8}\text{Se}_{0.2}$  (Fig. 3). For the single crystal X-ray

diffraction data refinement, a starting composition of  $\text{Hf}_{1.00}\text{As}_{1.00}(\text{As}_{0.79}\text{Se}_{0.21})$  was selected. The amount of Se and hence, the As/Se ratio was fixed to a fully occupied  $2c$  site, ascertained on the basis of the Se content determined by the chemical analyses. The final refinement, in which the occupancy factor of the  $2a$  site was varied, results in the following formula  $\text{Hf}_{1.00}\text{As}_{0.90(1)}(\text{As}_{0.79}\text{Se}_{0.21}) = \text{Hf}_{1.00}\text{As}_{1.69(1)}\text{Se}_{0.21}$ . The obvious deficiency of arsenic on site  $2a$  is in excellent agreement with the results of WDXS and the chemical analyses [4].

Silicon was also quantified by chemical analysis as an impurity component. One may speculate about a possible occupation of the vacancies within the arsenic layer, which would lead to the composition  $\text{As}_{0.9}\text{Si}_{0.1}$  on site  $2a$ . Clearly, this crystallographic position can be assumed to show a preferred tendency for occupation by any silicon impurity due to chemical considerations as already reported for the related compound  $\text{Hf}(\text{Si}_{0.5}\text{As}_{0.5})\text{As}$  [10]. This assumption, however, has to be checked by further X-ray diffraction studies on single crystals that are free of silicon as an impurity component.

Although As and Se are basically indistinguishable with standard X-ray diffraction techniques, we have obtained clear evidence from analogous systems that there is no significant Se-amount occupying the  $2a$  site. This assumption is confirmed by neutron diffraction experiments on the isotopic compound  $\text{ZrAs}_{1.6-\delta}\text{Se}_{0.4}$  ( $\delta = 0.02(1)$ ). These data were best refined by a structure model with a pure arsenic layer (together with 2 % defects) and a mixed occupied As/Se site.

In order to verify the symmetry assignment to the crystal structure in more detail, high resolution synchrotron powder diffraction experiments on pulverized materials were performed. To remove stress and strain effects, the microcrystalline powders of the crushed crystals were additionally annealed at 993 K for several days, before the diffraction experiments were carried out. The data collected at the beamline ID31 (ESRF, Grenoble) with the wavelength  $\lambda = 39.987(1)$  pm confirmed the tetragonal metric with high resolution and showed very sharp reflections up to  $2\theta = 40^\circ$ . No indications for splitting or additional superstructure reflections were obtained.

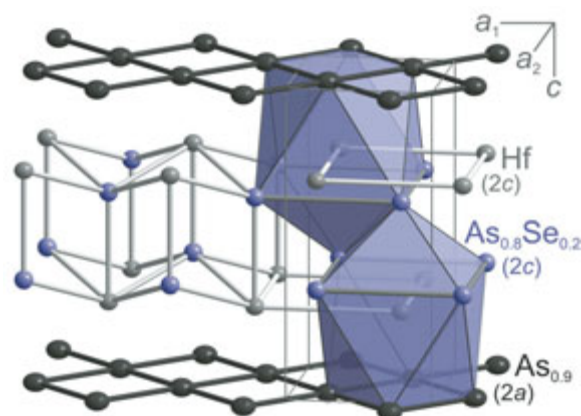


Fig. 3: Crystal structure of  $\text{HfAs}_{1.7}\text{Se}_{0.2}$ . Besides the arsenic layer  $\text{As}_{0.90(1)}$  ( $2a$ , black) and the mixed occupied site  $\text{As}_{0.8}\text{Se}_{0.2}$  ( $2c$ , blue), the coordination of Hf ( $2c$ , gray) is presented. The blue polyhedra represent mono-capped square-antiprisms built of five As/Se and four As atoms.

Although the crystal structures as well as the general crystal chemistry of  $\text{HfAs}_{0.90(1)}(\text{As}_{0.79}\text{Se}_{0.21})$  and  $\text{ZrAs}_{0.90(1)}(\text{As}_{0.5}\text{Se}_{0.5})$  are closely related [1], the composition range of the Hf compound clearly shifts to higher As-contents (i.e. less Se). Both compounds show metallic properties.

In contrast,  $\text{CeAsSe}$  [7] exhibits a narrow homogeneity range close to the 1:1:1 composition. For the Ce-compound, a distortion of the unit cell to an orthorhombic metric and the formation of infinite cis-trans chains of arsenic atoms was observed. No vacancies or positions of mixed occupancies were encountered. Yet, any small deviation from the ideal 1:1:1 composition severely reduces the orthorhombic distortion, probably by breaking the infinite As-chains into parts. To comprehend this behavior one has to take into account the semiconducting nature of  $\text{CeAsSe}$ .

### Summary of Characterization

The chemical composition of the title compound ( $\text{HfAs}_{1.7}\text{Se}_{0.2}$ ) was determined by various analytical methods. The analytical results are in excellent agreement. The contents of carbon, oxygen and iodine are below the limits of detection; impurities of Fe and Zr as impurities are present in traces, only.

Table 1: Summary of chemical and structural analyses

	Working			Crystal	
	Title	WDXS	ICP-OES	Structure	
Hf	1	1.000(3)	1.000(2)	1	2c
As	1.7	1.624(3)	1.66(2)	1.69(1) $\begin{pmatrix} 0.90(1) & 2a \\ 0.79^* & 2c \end{pmatrix}$	
Se	0.2	0.214(1)	0.215(5)	0.21*	2c
Si	0.94(5) wt.%		(LA-ICP-MS)		
C	< 0.03 wt.%		(C200)		
O	< 0.10 wt.%		(TCH600)		
I	< 0.02 wt.%		(CIC)		
Fe	0.10(3) wt.%		(ICP-OES)		
Zr	0.15(3) wt.%		(ICP-OES)		

\*) fixed parameters

The detected significant amount of silicon, which possibly occupies the crystallographic  $2a$  site ( $As_{0.90(1)}$ ), stems from the reaction ampoules. The focus of future investigations is aimed to produce large Si-free crystals and to verify the crystallographic preference of the Si. Currently, only tiny Si-free single crystals have been synthesized by using glassy carbon crucibles instead of carbon coated fused silica ampoules. These tiny crystals are not suitable for physical investigations.

### Physical Properties

In disordered metals, conduction electron scattering is intense and, hence, the motion of the charge carriers becomes diffusive rather than ballistic. The amount of disorder is generally quantified by the so-called disorder parameter defined as  $(k_F l_e)^{-1}$ , where  $k_F$  is the Fermi wavevector and  $l_e$  the electron mean free path. Weak and strong disorder correspond to  $(k_F l_e)^{-1} \ll 1$  and  $(k_F l_e)^{-1} \approx 1$ , respectively. In weakly disordered metals, each conduction electron is sensitive not only to the disorder potential but also to the electronic density fluctuations induced by other electrons. As a result, the energy levels are shifted and the thermodynamic and transport properties are modified. In particular, the resistivity shows a distinct  $T^{1/2}$  increase upon cooling. In general, the change in resistivity due to electron-electron interaction (EEI) could be of the same order of magnitude as the one caused by the scattering of the conduction electrons from TLS. Hence, the corrections to the resistivity stemming

from the former effects need to be extracted experimentally.

In the following, we will show that the electron-TLS interaction determines the *magnetic-field-independent*  $T^{1/2}$  term in the electrical resistivity, although the *magnetoresistivity* of  $HfAs_{1.7}Se_{0.2}$  may indeed be governed by EEI. Thermodynamic and transport properties of  $HfAs_{1.7}Se_{0.2}$  demonstrate that this material is a diamagnetic metal: (i) The DC magnetic susceptibility is temperature-independent and negative in a wide temperature range (not shown). (ii) The *Sommerfeld* coefficient of the electronic specific heat  $\gamma = 2.7 \text{ mJK}^{-2} \text{ mol}^{-1}$  [estimated from the  $B = 1 \text{ T}$  data (see inset in Fig. 4)] points to a relatively low density of states at the Fermi level. (iii) At temperatures above 12 K, both the electrical resistivity and the thermoelectric power show a quite common behavior, as displayed in Figs. 5 and 6, respectively. In addition,  $\rho(T)$  drops abruptly to zero when the temperature is decreased below 0.52 K. The sizeable specific heat jump  $\Delta c_p$  at  $T_c = 0.52 \text{ K}$  demonstrates that superconductivity is a bulk phenomenon in  $HfAs_{1.7}Se_{0.2}$ . As seen from Fig. 4, the superconducting transition is sharp ( $\Delta T_c = 0.04 \text{ K}$ ) indicating a good homogeneity of the investigated single crystal. The weak-coupling BCS prediction ( $\Delta c_p / \gamma T_c = 1.43$ ) yields  $\gamma \approx 2.0 \text{ mJK}^{-2} \text{ mol}^{-1}$ . This value is of the same order, but somewhat smaller, than the one experimentally observed (at  $B = 1 \text{ T}$ ).

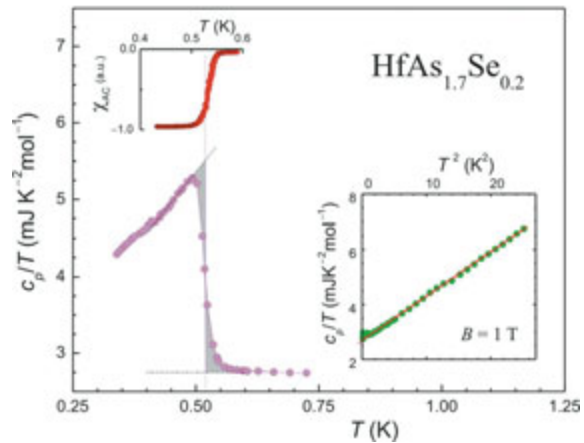


Fig. 4: Specific heat as  $c_p/T$  vs.  $T$  and AC magnetic susceptibility of  $HfAs_{1.7}Se_{0.2}$  in the vicinity of the superconducting transition. An equal-areas construction gives  $\gamma = 2.0 \text{ mJK}^{-2} \text{ mol}^{-1}$  and the superconducting critical temperature  $T_c = 0.52 \text{ K}$ . Inset: Fit of a  $\gamma T + \beta T^3$  dependence with  $\gamma = 2.7 \text{ mJK}^{-2} \text{ mol}^{-1}$  and  $\beta = 0.161 \text{ JK}^{-4} \text{ mol}^{-1}$  ( $\Theta_D = 330 \text{ K}$ ) to the heat capacity data at an overcritical magnetic field,  $B = 1 \text{ T}$ .

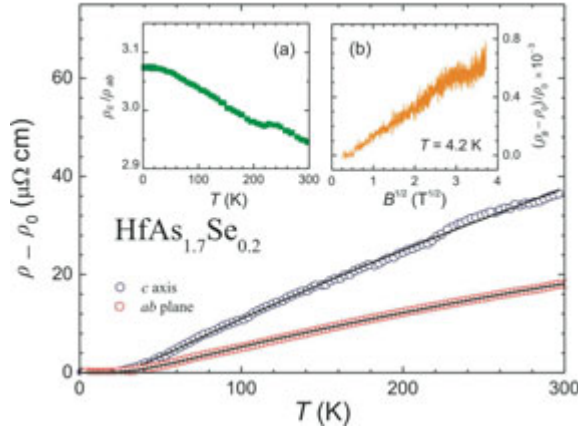


Fig. 5: Variation of the phonon contribution to the resistivity,  $\Delta\rho = \rho - \rho_0$ , with temperature for the  $\text{HfAs}_{1.7}\text{Se}_{0.2}$  single crystal. The values of the residual resistivity  $\rho_0$  are 143 and 426  $\mu\Omega\text{cm}$  in the  $ab$  plane and along the  $c$  axis, respectively. Solid lines indicate a best fit of a BGM relation to the experimental data. Inset (a): Temperature dependence of the electrical anisotropy ratio  $\rho_c/\rho_{ab}$ . Inset (b): Transverse magnetoresistivity  $(\rho_B - \rho_0)/\rho_0$  vs.  $B^{1/2}$ , measured along the  $c$  axis.

Fig. 5 displays the phonon contribution to the electrical resistivity,  $\Delta\rho = \rho - \rho_0$ , as a function of temperature for the  $\text{HfAs}_{1.7}\text{Se}_{0.2}$  single crystal measured along the main crystallographic directions. The tetragonal Hf based arsenide selenide displays moderate anisotropy, as highlighted by the room-temperature values of the residual resistivity  $\rho_0$ , 143 and 426  $\mu\Omega\text{cm}$  in the  $ab$  plane and along the  $c$  axis, respectively. In addition, the anisotropy factor  $\rho_c/\rho_{ab} \approx 3$  is only weakly temperature dependent below 300 K. The residual resistivity ratio is small ( $\text{RRR} \approx 1.1$ ) for both crystallographic directions. For  $T \geq 12$  K, the  $\Delta\rho$  term exhibits a temperature dependence which is well described by a generalized *Bloch-Grüneisen-Mott* (BGM) relation, as illustrated by the solid lines in Fig. 5. Such behavior is typically observed for rather disordered metals and indicates a significant structural disorder in this single crystal.

The thermopower  $S(T)$  of  $\text{HfAs}_{1.7}\text{Se}_{0.2}$  also confirms metallic conductivity (cf. Fig. 6, right axis). It exhibits an almost linear increase with positive slope up to a value of 11  $\mu\text{V}/\text{K}$  at room temperature. The positive sign of the thermopower is characteristic for the dominance of hole-like charge carriers. The small slope  $\alpha = S/T = 0.038 \mu\text{V}/\text{K}^2$  indicates good metallicity and a large Fermi energy  $E_F$  ( $\propto 1/\alpha$ )  $\approx 10^4$  K.

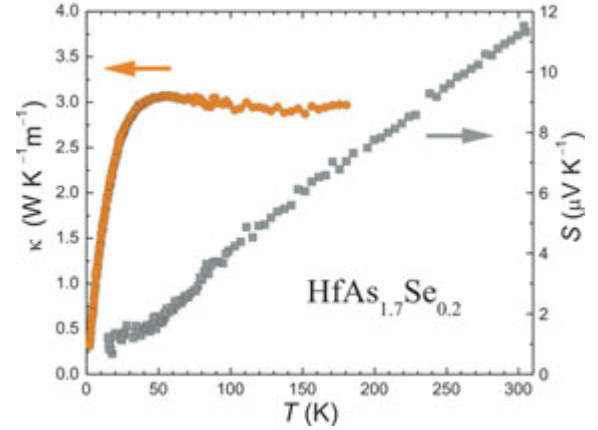


Fig. 6: Thermoelectric properties of  $\text{HfAs}_{1.7}\text{Se}_{0.2}$ . Left axis: thermal conductivity  $\kappa$  vs.  $T$ . Right axis: thermopower  $S$  vs.  $T$ .

The thermal conductivity of  $\text{HfAs}_{1.7}\text{Se}_{0.2}$  is also depicted in Fig. 6 (left axis). It exhibits low values of only 3  $\text{W}/\text{K}\text{m}$  with a broad maximum around 50 K. Due to radiation losses at temperatures above 150 K and, consequently, an overestimation of  $\kappa$ , only the low-temperature part is plotted. The almost glass-like  $T$ -dependence of the thermal conductivity provides evidence for dominating phonon scattering in a crystalline lattice caused by substantial elemental site exchange and vacancies.

Fig. 7 compares the  $c$ -axis electrical resistivity data measured on  $\text{HfAs}_{1.7}\text{Se}_{0.2}$  both in zero magnetic field and 14 T. These low-temperature results are presented as the relative change of the resistivity normalized to the corresponding value at 1 K,  $\Delta\rho/\rho_{1\text{K}}$ . Below about 12 K and in zero field, an extra  $-AT^{1/2}$  ( $A = 0.054 \mu\Omega\text{cm}/\text{K}^{1/2}$ ) term in the resistivity is resolved. Its magnitude increases with decreasing temperature down to around 0.85 K, below which superconducting fluctuations set in. It is remarkable that the amplitude of the low- $T$  upturn remains unchanged in  $B = 14$  T. Such a behavior, *i.e.*, a magnetic-field-independent  $-AT^{1/2}$  term in the resistivity appears to be a common feature in many PbFCl-type arsenide selenides. Most interestingly, however, for  $B = 14$  T we observe a saturation of  $\rho(T)$  below  $T_{\text{sat}} \approx 0.49$  K. A similar, but somewhat less pronounced, saturation has also been found for  $\text{ThAsSe}$  [3], but has not yet been explained. For the tetragonal compound  $\text{HfAs}_{1.7}\text{Se}_{0.2}$ , the disorder parameter can be calculated from the free-electron formula  $(k_F l_e)^{-1} = \hbar/3m_e D$ , where  $D$  is the electron diffusion constant.

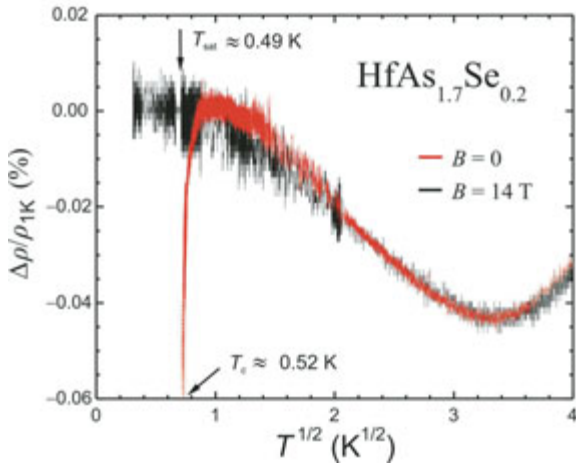


Fig. 7: Low-temperature electrical resistivity of  $\text{HfAs}_{1.7}\text{Se}_{0.2}$  as  $\Delta\rho/\rho_{1\text{K}}$  at zero field and 14 T. The electrical current and the magnetic field were applied in the directions parallel and perpendicular to the  $c$  axis, respectively.

For the  $c$  axis, we estimated  $D \approx 0.6 \text{ cm}^2\text{s}^{-1}$ , using the Einstein relation  $D^{-1} = \rho_0 e^2 N(0)$ . Here,  $\rho_0$  is the residual resistivity and  $N(0)$  the density of states at the Fermi level calculated from the electronic specific heat. Within this formalism we obtained  $(k_{\text{F}}l_{\text{e}})^{-1} \approx 0.6$  which points to strong rather than weak disorder. Therefore, a perturbation treatment of the disorder should not be used for  $\text{HfAs}_{1.7}\text{Se}_{0.2}$ . On the one hand, however, the magnetoresistivity is positive and obeys a  $B^{1/2}$  behavior in the whole field range [see inset (b) in Fig. 5]. Such a positive  $B^{1/2}$  magnetoresistivity may be described to some EEI effects. On the other hand, the latter could not be resolved in our  $\rho(T)$  experiment, because (i) the measurements were performed for  $g\mu_{\text{B}}H$  greater than  $k_{\text{B}}T$  and (ii)  $\text{HfAs}_{1.7}\text{Se}_{0.2}$  is a system with low diffusion constant. In the case that both the zero-field  $T^{1/2}$  correction in  $\rho(T)$  and the positive  $B^{1/2}$  magnetoresistivity were due to the EEI in the diffusion channel, one could estimate the interaction constant  $F_{\text{d}}$ , which depends on the details of the electron screening and the Fermi surface of the conductor under consideration. ( $F_{\text{d}}$  varies from 1 to 0 for complete and no screening, respectively.) Combining eqs. 3.41-3.43 in Ref. [11] with our experimental data for  $T = 1 \text{ K}$  and  $B = 14 \text{ T}$ , we obtain  $F_{\text{d}} \approx 0.45$  for  $\text{HfAs}_{1.7}\text{Se}_{0.2}$ . According to [11], application of an external field of 14 T should lead to an easily detectable resistivity change of about 30 % at the lowest temperatures. Obviously, this is not the case for  $\text{HfAs}_{1.7}\text{Se}_{0.2}$  and, hence, the EEI should be ruled out as a source of the magnetic-

field-independent  $-AT^{1/2}$  term in the resistivity. Finally, we note that, while a  $-AT^{1/2}$  behavior was also observed in the related systems Th-As-Se [3] and Zr-As-Se [1], in the latter cases the  $B^{1/2}$  magnetoresistivity is negative at  $B > 1 \text{ T}$  as well as 4 T. The different sign of the magnetoresistivity of different PbFCl type of structure arsenide selenides calls for further investigations.

## Summary

Large single crystals of  $\text{HfAs}_{1.7}\text{Se}_{0.2}$  were grown by chemical transport reaction using iodine as transport agent. The chemical composition of the crystals was characterized in detail by various analytical methods. The results of the crystal structure investigations using X-ray and synchrotron radiation diffraction techniques reveal a tetragonal PbFCl (ZrSiS) type of structure with a partially unoccupied  $2a$  site ( $\text{As}_{0.9}$ ) and a mixed occupancy on the  $2c$  site ( $\text{As}_{0.8}\text{Se}_{0.2}$ ). Thus, the Hf based compound exhibits similar structural features as observed for  $\text{ZrAs}_{1.4}\text{Se}_{0.5}$  and is the second representative of non-actinide-containing compounds revealing non-magnetic Kondo behavior.

$\text{HfAs}_{1.7}\text{Se}_{0.2}$  is a diamagnetic metal which exhibits superconductivity at  $T_{\text{c}} = 0.52 \text{ K}$ . Several parameters, e.g., a low electron-diffusion constant  $D \approx 0.6 \text{ cm}^2\text{s}^{-1}$  and a small disorder parameter  $(k_{\text{F}}l_{\text{e}})^{-1} \approx 0.6$ , point to strong disorder in the single crystalline  $\text{HfAs}_{1.7}\text{Se}_{0.2}$  sample. Similar to other PbFCl type arsenide selenides, the Hf based compound displays a magnetic-field-independent  $-AT^{1/2}$  term in the low-temperature electrical resistivity. This extra term presumably originates from the electron scattering off structural two-level systems. The positive sign of the magneto-resistivity being proportional to  $B^{1/2}$  may be caused by electron-electron-interactions.

We would like to thank Dr. Ulrich Burkhardt, Monika Eckert, and Petra Scheppan (EDXS/ WDXS analyses, metallography), Anja Völzke, Martina Seibt, Ulrike Schmidt (ICP-OES, CGHE); Sebastian Schwinger (CIC), Jana Buder (SEM image), Thomas Bauer (TTO) as well as Dr. Stefan Hoffmann, and Susann Müller (DSC, DTA/TG). Technical support by Irene Margiolaki at the beamline ID31 (ESRF, Grenoble) is also gratefully acknowledged.

## References

- [1] *M. Schmidt, T. Cichorek, R. Niewa, A. Schlechte, Yu. Prots, F. Steglich, and R. Kniep*, *J. Phys.: Condens. Matter* **17** (2005) 5481.
- [2] *T. Cichorek, D. Gnida, R. Niewa, A. Schlechte, M. Schmidt, Yu. Prots, R. Ramlau, Z. Henkie, R. Kniep, and F. Steglich*, *J. Low Temp. Phys.* **147** (2007) 309.
- [3] *T. Cichorek, A. Sanchez, P. Gegenwart, F. Weickert, A. Wojakowski, Z. Henkie, G. Auffermann, S. Paschen, R. Kniep, and F. Steglich*, *Phys. Rev. Lett.* **94** (2005) 236603.
- [4] *A. Schlechte, R. Niewa, M. Schmidt, H. Borrmann, G. Auffermann, and R. Kniep*, *Z. Kristallogr. NCS* **222** (2007) 369.
- [5] *A. Schlechte, R. Niewa, T. Cichorek, Yu. Prots, M. Schmidt, R. Ramlau, and R. Kniep*, *Z. Anorg. Allg. Chem.* **623** (2006) 2107.
- [6] *A. Schlechte, R. Niewa, M. Schmidt, G. Auffermann, Yu. Prots, W. Schnelle, D. Gnida, T. Cichorek, F. Steglich, and R. Kniep*, *Sci. Technol. Adv. Mat.* **8** (2007) 341.
- [7] *A. Schlechte, R. Niewa, Yu. Prots, W. Schnelle, M. Schmidt, and R. Kniep*, *Inorg. Chem.* **48** (2009) 2277.
- [8] *J. Schoenes, R. L. Withers, and F. Hulliger*, *J. Magn. Magn. Mater.* **310** (2007) 1778.
- [9] *Z. Henkie, A. Pietraszko, A. Wojakowski, L. Kępiński, and T. Cichorek*, *J. Alloy. Compd.* **317-318** (2001) 52.
- [10] *A. P. Grosvenor, R. G. Cavell, A. Mar, and R. I. R. Blyth*, *J. Solid State Chem.* **180** (2007) 2670.
- [11] *P. A. Lee, and T. V. Ramakrishnan*, *Rev. Mod. Phys.* **57** (1985) 287.

<sup>1</sup> Institute of Low Temperature and Structure Research, Polish Academy of Sciences, Wrocław, Poland

<sup>2</sup> Department Chemie, Technische Universität München, Garching, Germany